Mantle dynamics of continent-wide Cenzoic subsidence and tilting of Australia

Lydia DiCaprio[1*], Michael Gurnis[2], R. Dietmar Müller[1], Eh Tan[3+]

[1] EarthByte Group, School of Geosciences, Madsen Building F09, The University of Sydney, NSW 2006, Australia

[2]Seismological Laboratory, California Institute of Technology, Pasadena CA 91125, USA

[3]Computational Infrastructure for Geodynamics, California Institute of Technology, Pasadena CA 91125, USA

[+]Now at: Institute for Geophysics, University of Texas, Austin, TX 78712, USA

[*] Now at: ExxonMobil Exploration Company, Houston TX, USA

Corresponding Author: Lydia.DiCaprio@ExxonMobil.com

In press,

Lithosphere

ABSTRACT

Australia is distinctive as it experienced first order, broad-scale vertical motions during the Cenozoic. Here we use plate tectonic reconstructions and a model of mantle convection to quantitatively link the large-scale flooding history of the continent to mantle convection since 50 Ma. Subduction-driven geodynamic models show that Australia undergoes a 200 m northeast downward tilt as it approaches and overrides subducted slabs between Melanesia and the proto-Tonga Kermadec subduction systems. However, only if we assume that Australia has moved northward away from a relatively hot mantle anomaly does the model produce the observed continent-wide subsidence with 300 m of northeast downward tilt since the Eocene. The models suggest that Australia's paleo-shoreline evolution can only be reproduced if the continent moved northward, away from a large buoyant anomaly. This results in continent wide subsidence of about 200 m. The additional progressive, continent-wide tilting down to the northeast can be attributed to the horizontal motion of the continent towards subducted slabs sinking below Melanesia.

1. Introduction

Dynamic topography is an important control on the Earth's overall topography and the gravity field [*Cazenave et al.*, 1989; *Christensen*, 1998; *Colin and Fleitout*, 1990; *Hager et al.*, 1985; *LeStunff and Ricard*, 1995]. An intriguing implication of this concept is the contribution of mantle processes towards the formation of intra-continental basins, which may be recorded by continental flooding [*Artemieva*, 2007; *Gurnis*, 1990; *Mitrovica et al.*, 1989; *Pysklywec and Mitrovica*, 1998; *Spasojević*, 2008]. Although mantle driven topography on continents is a global phenomenon [*Heine et al.*, 2008], it is generally difficult to quantitatively link continental geology to mantle processes and to resolve the dynamic component of amplitude and rate of change. This is largely due to our limited ability to separate a dynamic component of topography from other crustal and lithospheric processes. In addition, geodynamic models are limited by their input conditions and their ability to produce realistic magnitudes of dynamic topography to match surface observations [*Billen et al.*, 2003].

While it may be difficult to isolate the mantle-driven topography from changes in lithospheric and crustal thickness [*Wheeler and White*, 2000], Australia is generally free from such difficulties since it is a stable continent with distal plate boundaries (**Figure 1**). However, since the Eocene, rapid sea floor spreading on the South East Indian Ridge moved the Australian continent away from Antarctica and toward the subduction zones in SE Asia. Indeed, despite the absence of proximal plate boundaries, it has been suggested that Australia has undergone both a broad scale subsidence since the Late Cretaceous [*Bond*, 1978; *DiCaprio et al.*, 2009; *Russell and Gurnis*, 1994] and a progressively increasing northeast downward tilt since the Eocene [*DiCaprio et al.*, 2009; *Sandiford*, 2007; *Sandiford et al.*, 2009]. Broad scale subsidence of the continent is inferred from the difference between relative and global sea level. As global sea level fell since the Cretaceous [*Haq et al.*, 1987; *Haq and Al-Qahtani*, 2005; *Miller et al.*, 2005], Australia became increasingly flooded. The preserved marine facies imply that the entire continent experienced approximately a 200 m downward shift since the Cretaceous [*Bond*, 1978; *DiCaprio et al.*, 2009; *Russell and Gurnis*, 1994; *Veevers*, 2000]. In addition to the broad scale subsidence, differential vertical motion of the continent since the Cenozoic inferred from reconstructed shorelines shows that the Australian continent was progressively tilted down towards the northeast by around 300 m since the Eocene [*DiCaprio et al.*, 2009] (**Figure 1**).

The downward shift and progressive tilting of Australia remain unexplained geodynamically. Here, for the first time, we attempt to interpret these first order features in the stratigraphic record with geodynamic models. Moreover, to overcome the limitations of earlier geodynamic models [*Gurnis et al.*, 1998; *Gurnis and Müller*, 2003], we include a more realistic lithosphere through the assimilation of tectonic boundary conditions. Our geodynamic models include the history of plate motions, changing plate geometries and modeled ages and thermal structures of the subducting lithosphere to investigate the time-dependent dynamically driven topography of the southwest Pacific and Australia since the Eocene. Surprisingly, we find that the subduction control on the vertical motions of Australia is insufficient to explain the continent-wide subsidence observed in paleo-shoreline analysis.

2. Model Setup

We use continuously changing plate velocities and plate margins on 1 Myr increments as surface velocity boundary conditions [*Gurnis et al.*, 2010]. Ocean floor paleo-age grids [*Müller et al.*, 2008] constrain the lithospheric temperature profile. We embed a high-resolution regional model within a low-resolution global model using nested *CitcomS* solvers [*Tan et al.*, 2006] and incompressible flow. The nested solver allows us to compute the model in a high-resolution regional grid with a flow-through boundary condition, which avoids the artifact in dynamic topography caused by return flow within a confined box. The regional model has more than 4 times the lateral resolution of the global models resolving features at 64 km in longitude and 40 km in latitude. The radial resolution of the regional model is 33 km to a depth of 2250 km. We use active tracers within the continental lithosphere to mimic chemical buoyancy and within the mantle wedge to lower the viscosity [*Manea and Gurnis*, 2007]. For more information about the method and data assimilation see online supplementary material and DiCaprio [2009].

Our models have a Newtonian viscosity that is dependent on temperature, depth, composition and position. The mantle is divided into four layers: lithosphere (0-100 km), astehnosphere (100-410 km), transition zone (410-670 km), and lower mantle (670-2880 km). All models have the same radial distribution of viscosity (**Table 1**), however models with alternative layered viscosities were examined further in DiCaprio [2009]. We varied both the strength of the asthenosphere and lower mantle. Our preferred models have a weak asthenosphere [2×10^{20} Pas] and strong lower mantle. The weak asthenosphere allowed subducted slabs to be more easily distributed laterally within the upper mantle beneath the Australian northeast margin and produce a broader topographic signal compared to those with a higher viscosity upper mantle. Models with a high viscosity lower mantle (1×10^{23} Pas) impede the descent of slabs into the lower mantle. These models retain more cool material in the upper mantle and produce a smaller amplitude but broad scale length of dynamic topography. Here we show the effect of changes in the gradient of the Clapeyron slope for the phase changes bounding the mantle transition zones were altered for a range of reasonable values based on mineral physics experiments (**Table 2**), as summarized in Billen [2008].

3. RESULTS

Our models show that since the Eocene subducted material has accumulated beneath the northeastern margin of Australia and the Tasman Sea (**Figure 2**). In the model, slabs presently beneath the northeast Australian margin are the product of Melanesian subduction, while those beneath the Tasman Sea are remnants of Loyalty-Tonga-Kermadec subduction. This result is consistent with fast velocity perturbations observed beneath the NE margin in tomography [*Hall and Spakman*, 2003; *Ritsema et al.*, 1999]. Between 50 and 32 Ma, slabs from Melanesian and Loyalty subduction descend through the upper mantle and are laid flat within the transition zone more than 2000 km away from the trench. At this time dynamic topography affecting the Australian continent is negligible while dynamic topography amplitudes of several hundred meters of subsidence are concentrated within the back-arc regions (**Figure 2**). However, between 32 and 10 Ma a long wavelength component of dynamic topography develops as Australia begins to drift over the slabs accumulated within the transition zone. This causes subsidence of up to 100 m along the northeastern Australian margin between 32 and 10 Ma. Between 10 and 2 Ma, the slabs whose descent was partially impeded by the phase transition at 660 km depth, start to pass through the 660 km phase boundary into the lower mantle. This results in up to 200 m of total dynamic subsidence on the north and northeastern Australian margin corresponding with the timing of northeastern margin reef demise [*DiCaprio et al.*, 2010; *Isern et al.*, 2002].

Since the continent experiences little vertical disturbance at 50 Ma (Figure 2), its topography at 50 Ma is a good proxy of iso-static topography. Differential topography is computed as the change relative to the initial topography at 50 Ma, a quantity that can be compared directly against the anomalous subsidence and tilting of the continent recovered through an analysis of paleo-shorelines [*DiCaprio et al.*, 2009]. A SW-NE cross-section shows the slope of the modeled subsidence across the continent poorly matches the slope from paleo-shoreline analysis since the Miocene (**Figure 3**). Although, the modeled subsidence is qualitatively consistent with the trend observed by paleo-shoreline analysis, the modeled subsidence is much too confined to the north. Both models and paleo-shoreline analysis show that since the Cenozoic Australia has subsided in the northeast and the magnitude of this subsidence has increased towards the present.

The model which best approximates the subsidence estimated by paleo-shoreline analysis has a steep Clapeyron slope (4 MPa/K) at the 410 km discontinuity and a shallow Clapeyron slope (2 MPa/K) at the 660 km discontinuity (**Figure 3**). The shallow

Clapeyron slope at the 660 km phase change allows slab material to descend into the lower mantle relatively easily and produces a larger signal of surface subsidence in the northeast.

Vertical subsidence of Australia during the Cenozoic

Our models produce insufficient surface subsidence since the Miocene, approximately 100 m smaller than inferred from paleo-shoreline analysis. This implies that the continent requires an additional downward shift over a much longer wavelength since the Oligocene. The downward shift of the Australian continent may be related to its motion northward away from putatively hot or chemically buoyant mantle beneath Antarctica.

The mantle beneath Cenozoic Antarctica may have been relatively hot due to its connection to Gondwanaland. This is inferred from the abundance of magmatism before and during breakup [*Kent*, 1991; *Storey et al.*, 1995]. The presence of a large-scale upwelling beneath Antarctica during the Cenozoic and today is consistent with the distribution and geochemistry of igneous rocks [*Behrendt et al.*, 1991; *Finn et al.*, 2005; *LeMasurier and Landis*, 1996; *Sutherland et al.*, 2010]. In addition, global tomography models reveal low velocity perturbations in the upper mantle and transition zone beneath the West Antarctic margin [*Grand*, 2002; *Gu et al.*, 2001; *Masters et al.*, 2000; *Ritsema and Heijst*, 2000]. Recently, geodynamic models showed that the Campbell Plateau subsided by about 1 km as it moved away from a buoyant mantle anomaly presently located beneath Antarctica [*Spasojevic et al.*, 2010; *Sutherland et al.*, 2010]. These observations and interpretations suggest that Australia has likely also moved away from a dynamic topography high since 50 Ma.

Motivated by these observations, we modified model named M50_1 by prescribing a 5% temperature difference (75 °C hotter) difference in the mantle beneath Australia and Antarctica. The buoyancy associated with this hot mantle causes a topographic high beneath both continents at 50 Ma. However, as the spreading rate at the South East Indian Ridge increases and accelerates Australia northward, the Australian continent moves away from this topographic high (Appendix Figure A1). This motion causes vertical subsidence of the whole continent in addition to a downward tilt towards the northeast as the continent overrides the Melanesian subducted slabs. The summation of these two dynamic forces matches the predicted tilt of the continent from paleo-shoreline analysis (**Figure 3**). The buoyant mantle produces the additional broad scale subsidence required to fit the paleo-shoreline analysis. This can be seen by computing a residual since the Miocene (**Figure 4**C) between the modeled differential topography (**Figure 4** A) and the anomalous topography from paleo-shorelines (**Figure 4** B). However, we would like to note that the mantle buoyancy here modeled as simply a thermal effect, is likely due to a combination of mantle hydration, and other geochemical and thermal heterogenieities that may be associated with the long-lived eastern Gondwanaland slab graveyard [*Spasojevic et al.*, 2010].

Conclusions

Dynamic topography from models of the evolution of subducted slabs since the Eocene are in disagreement with geologic observations of continent-scale tilting. Models with the negative thermal buoyancy associated with slabs between Melanesia and the proto-Tonga Kermadec subduction systems only recover the tilt of the continent, while the vertical motion of the continent is underestimated by up to 200 m. By including 75°C (5%) hotter than average mantle beneath the Australian and Antarctic continent our models match both the tilt and vertical displacement of the Australian continent. The agreement of the models with Australia's paleo-shoreline evolution suggest that the mantle anomaly was buoyant and it may be the result of mantle hydration or some combination of thermal and geochemical heterogeneities. During the Cenozoic, as spreading along the South East Indian Ridge accelerated Australia away from the buoyant Antarctic mantle and towards the subduction zones in Melanesia the continent both subsided in bulk and tilted to the NE.

ACKNOWLEDGEMENTS

We are thankful to Leif Strand from the CIG for his assistance with CitcomS. The Australian Research Council Australian Postgraduate Award administered by the University of Sydney with additional support from NSF EAR-0810303 financially supported Lydia DiCaprio. This work represents contribution 10022 of the Division of Geological and Planetary Sciences, California Institute of Technology.

Figures

Figure 1: Topography and bathymetry [*Amante and Eakins*, 2008] of the Australian region showing contours of dynamic topography estimated from analysis of paleo-shorelines [*DiCaprio et al.*, 2009], present day plate boundaries [*Bird*, 2003] and areas discussed in the text. Data distribution used for the paleo-shoreline analysis is shown in appendix figure 2.

Figure 2: Surface dynamic topography (left) since the Eocene shows progressively increasing subsidence in the northeast of Australia as the continent drifts towards the subduction zones. Reconstructed continents and plate boundaries show the position of fossil subduction zones since the Eocene. Temperature cross-sections (right) since the Eocene shows slabs accumulating beneath the northeastern margin of Australia and beneath the Tasman Sea. Temperature cross-sections are plotted with non-dimensional depths and are overlain by the 660 and 410 phase changes, which are deflected by temperature anomalies.

Figure 3: A comparison of profiles of differential topography from geodynamic models (colored lines) and paleo-shoreline analysis (grey lines) [*DiCaprio et al.*, 2009]. Differential topography is sampled from along a line running SW to NE shown in the lower right. The profiles are for selected times since the Eocene and differential topography refers to the change in subsidence since an Eocene reference state. All geodynamic models show an increase in tilt toward the NE since the Eocene, which is

consistent with the trend observed from paleo-shorelines. However the model with the hotter mantle (orange line) shows is a good match to both the trend and total differential topography observed through paleo-shoreline analysis.

Figure 4: Column (A) shows modeled differential subsidence since 50 Ma. Forward geodynamic models were initiated at 50 Ma, the approximate timing of major plate reorganization in the SW Pacific [*Whittaker et al.*, 2007]. Column (B) shows differential subsidence since 44 Ma from geologic and paleo-shoreline analysis [*DiCaprio et al.*, 2009]. The 44 Ma reference time and subsequent intervals 33Ma, 8Ma and 4Ma are constrained by the available paleogeographic reconstructions (described in Dicaprio et al [2009]). Column (C) shows the residual between column A and B. Residuals were calculated using the geodynamic model timesteps closest to the paleogeographic reconstructions. Columns A and B show the evolution of the tilting of the Australian continent through time. The residual (C) is mostly flat over the Australian continent and has an approximate misfit of 100 m. This indicates that the Australian continent has experienced 100 m of subsidence that is not accounted for by our geodynamic models. Shaded contours are at 100m intervals for all plots.

Tables

Table 1: Parameters held constant within the models

Parameter	Notation	value
Reference mantle density	ρ_0	$3500\, kg/m^3$
Gravity	g	$10\, m/s^2$
Temperature of the surface	T_0	$0\,°C$
Change in temperature from the core mantle boundary to the surface	$\Delta\mathrm{T}$	$1500\,°C$
Radius	R_0	$6371000\, m$
Coefficient of thermal expansion	α	$2\times10^{-5}\ K^{-1}$
Thermal diffusivity	κ	$1\times10^{-6}\ m^2/s$
Reference viscosity	η_0	$2\times10^{21}\ Pas$
Viscosity: lithosphere (0-100 km)	η_{lith}	$2\times10^{23}\ Pas$
Viscosity: asthenosphere (100 - 410 km)	η_{asth}	$2\times10^{20}\ Pas$
Viscosity: transition zone (410-660 km)	η_{trans}	$1\times10^{22}\ Pas$
Viscosity: lower mantle (660 – 2800 km)	η_{LM}	$1\times10^{23}\ Pas$
Rayleigh number	$R_a = \frac{\rho_0 g \alpha_0 \Delta\mathrm{T} R_0^3}{\kappa_0 \eta_0}$	$R_a = 1.3576\times10^{+08}$

Table 2: Geodynamic models and properties

Model Name	Slope 410 (MPa/K)	Slope 660 (MPa/K)

M50_1	4	-2
M50_2	4	-4
M50_3	2	-4
M50_4	2.9	-3
AUS_Hot	4	-2

REFERENCES

Amante, C., and B. W. Eakins (2008), ETOPO1 1 Arc-Minute Global Relief Model: Procedures, Data Sources and Analysis, National Geophysical Data Center, edited, NESDIS, NOAA, U.S. Department of Commerce, Boulder, CO.

Artemieva, I. M. (2007), Dynamic topography of the East European craton: Shedding light upon lithospheric structure, composition and mantle dynamics, *Global and Planetary Change*, *58*(1-4), 411-434.

Behrendt, J. C., et al. (1991), Geophysical studies of the West Antarctic Rift System, *Tectonics*, *10*, 1257–1273.

Billen, M. (2008), Modeling the dynamics of subduction slabs, *Annual Review of Earth and Planetary Sciences*, *36*, 325-356.

Billen, M. I., et al. (2003), Multiscale dynamics of the Tonga–Kermadec subduction zone, *Geophysical Journal International*, *153*, 359-388.

Bird, P. (2003), An updated digital model of plate boundaries, *Geochemistry Geophysics Geosystems*, *4*(3).

Bond, G. C. (1978), Speculations on real sea-level changes and vertical motions of continents at selected times in the Cretaceous and Tertiary Periods, *Geology*, *6*, 247-250.

Cazenave, A., et al. (1989), Global coupling of Earth surface topography with hotspots, geoid and mantle heterogeneities., *Nature*, *340*, 54–57.

Christensen, U. R. (1998), Dynamic phase boundary topography by latent heat effects, *Earth and Planetary Science Letters*, *154*, 295–306.

Colin, P., and L. Fleitout (1990), Topography of the ocean floor: thermal evolution of the lithosphere and interaction of mantle heterogeneities with the lithosphere., *Geophysical Research Letters*, *11*, 1961–1964.

DiCaprio, L. (2009), The Geodynamic history of the Australian region since the Cretaceous, PhD thesis, 182 pp, University of Sydney, Sydney.

DiCaprio, L., et al. (2009), Long-wavelength tilting of the Australian continent since the Late Cretaceous, *Earth and Planetary Science Letters*, *278*, 175-185.

DiCaprio, L., et al. (2010), A dynamic process for drowning carbonate reefs on the Northeastern Australian margin *Geology*, *38*, 11-14.

Finn, C. A., et al. (2005), A Cenozoic diffuse alkaline magmatic province (DAMP) in the southwest Pacific without rift or plume origin, *Geochemistry Geophysics Geosystems*, *6*(1).

Grand, S. P. (2002), Mantle shear-wave tomography and the fate of subducted slabs, *Phil. Trans. R. Soc. Lond.*, *Ser. A 360*, 2475–2491.

Gu, Y. J. A., et al. (2001), Models of the mantle shear velocity and discontinuities in the pattern of lateral heterogeneities, *Journal of Geophysical Research*, *106*(11), 11169-11199.

Gurnis, M. (1990), Bounds on global topography from Phanerozoic flooding of continental platforms, *Nature*, *344*, 754-756.

Gurnis, M., et al. (1998), Cretaceous vertical motion of Australia and the Australian-Antarctic discordance, *Science*, *279*(5356), 1499-1504.

Gurnis, M., and R. D. Müller (2003), The Origin of the Australian Antarctic Discordance, in *Evolution and Dynamics of the Australian Plate*, edited by R. R. Hillis and R. D. Müller, pp. 417-430, Sydney.

Gurnis, M., et al. (2010), Global Plate Reconstructions with Continuously Closing Plates, *Geochemistry, Geophysics, Geosystems submitted*, *Special theme "Plate Reconstructions, Mantle Convection, and Tomography Models: A Complementary Vision of Earth's Interior"*(In review).

Hager, B. H., et al. (1985), Lower mantle heterogeneity, dynamic topography and the geoid, *Nature*, *313* 541–545.

Hall, R., and W. Spakman (2003), Mantle structure and tectonic evolution of the region north and east of Australia, in *Evolution and Dynamics of the Australian Plate*, edited by H. R.R. and M. R.D., pp. 361-382, Geological Society of Australia, Sydney.

Haq, B. U., et al. (1987), Chronology of fluctuating sea levels since the Triassic, *Science*, *235*, 1156-1167.

Haq, B. U., and M. Al-Qahtani (2005), Phanerozoic cycles of sea-level change on the Arabian Platform, *GeoArabia*, *10*(2), 127-160.

Heine, C., et al. (2008), Subsidence in intracontinental basins due to dynamic topography, *Physics of the Earth and Planetary Interiors*, *171*, 252–264.

Isern, A. R., et al. (2002), Volume 194 Initial Reports: Constraining Miocene sea level change from carbonate platform evolution, Marion Plateau, Northeast Australia, Sites 1192–1199, Ocean Drilling Program.

Kent, R. (1991), Lithospheric uplift in eastern Gondwana: Evidence for a long-lived mantle plume system?, *Geology*, *19*, 19-23.

LeMasurier, W. E., and C. A. Landis (1996), Mantle-plume activity recorded by low relief erosion surfaces in West Antarctica and New Zealand., *Geological Society of America Bulletin*, *108*, 1450-1466.

LeStunff, Y., and Y. Ricard (1995), Topography and geoid due to lithospheric mass anomalies, *Geophysical Journal International*, *122*, 982–990.

Manea, V., and M. Gurnis (2007), Subduction zone evolution and low viscosity wedges and channels, *Earth and Planetary Science Letters*, *264*, 22–45.

Masters, G., et al. (2000), The Relative Behavior of Shear Velocity, Bulk Sound Speed, and Compressional Velocity in the Mantle: Implications for Chemical and Thermal Structure", in *Earth's Deep Interior*, edited by S. Karato, et al., AGU Monograph 117, AGU, Washington D.C.

Miller, K. G., et al. (2005), The phanerozoic record of global sea-level change, *Science*, *310*(5752), 1293-1298.

Mitrovica, J. X., et al. (1989), Tilting of Continental Interiors by the Dynamical Effects of Subduction, *Tectonics*, *5*, 1078–1094.

Müller, R. D., et al. (2008), Long-Term Sea-Level Fluctuations Driven by Ocean Basin Dynamics, *Science*, *319*(5868), 1357 - 1362.

Pysklywec, R. N., and J. X. Mitrovica (1998), Mantle flow mechanisms for the large-scale subsidence of continental interiors, *Geology*, *26*(8), 687-690.

Ritsema, J., et al. (1999), Complex shear wave velocity structure imaged beneath Africa and Iceland, *Science*, *286*(5446), 1925-1928.

Ritsema, J., and H. J. v. Heijst (2000), Seismic imaging of structural heterogeneity in Earth's mantle: evidence for large-scale mantle flow, *Science Progress*, *83*, 243-259.

Russell, M., and M. Gurnis (1994), The planform of epeirogeny: vertical motions of Australia during the Cretaceous, *Basin Research*, *6*, 63–76.

Sandiford, M. (2007), The tilting continent: A new constraint on the dynamic topographic field from Australia, *Earth and Planetary Science Letters*, *261*(1-2), 152-163.
Sandiford, M., et al. (2009), Tectonic framework for the Cenozoic cratonic basins of Australia *Australian Journal of Earth Sciences 56*(S5–S18).
Spasojevic, S., et al. (2010), Inferring mantle properties with an evolving dynamic model of the Antarctica-New Zealand region from the Late Cretaceous, *Journal of Geophysical Research*, *115*(B05402, doi:10.1029/2009JB006612), 16.
Spasojević, S., L. Liu, M. Gurnis, and R. D. Müller (2008), The case for dynamic subsidence of the U.S east coast since the Eocene, *Geophysical Research Letters*, *35*(L08305).
Storey, M., et al. (1995), Timing of hot spot-related volcanism and the breakup of Madagascar and India, *Science*, *267*, 852-855.
Sutherland, R., et al. (2010), Mantle upwelling after Gondwana subduction death explains anomalous topography and subsidence histories of eastern New Zealand and West Antarctica, *Geology*, *38*(2), 155-158.
Tan, E., et al. (2006), GeoFramework: Coupling multiple models of mantle convection within a computational framework, *Geochemistry, Geophysics, Geosystems 7*.
Veevers, J. J. (2000), *Billion-year earth history of Australia and neighbours in Gondwanaland*, 388 pp., GEMOC Press, North Ryde, N.S.W.
Wheeler, P., and N. White (2000), Quest for dynamic topography: Observations from Southeast Asia, *Geology*, *28*(11), 963-966.
Whittaker, J., et al. (2007), Major Australian-Antarctic plate reorganization at Hawaiian-Emperor bend time, *Science*.

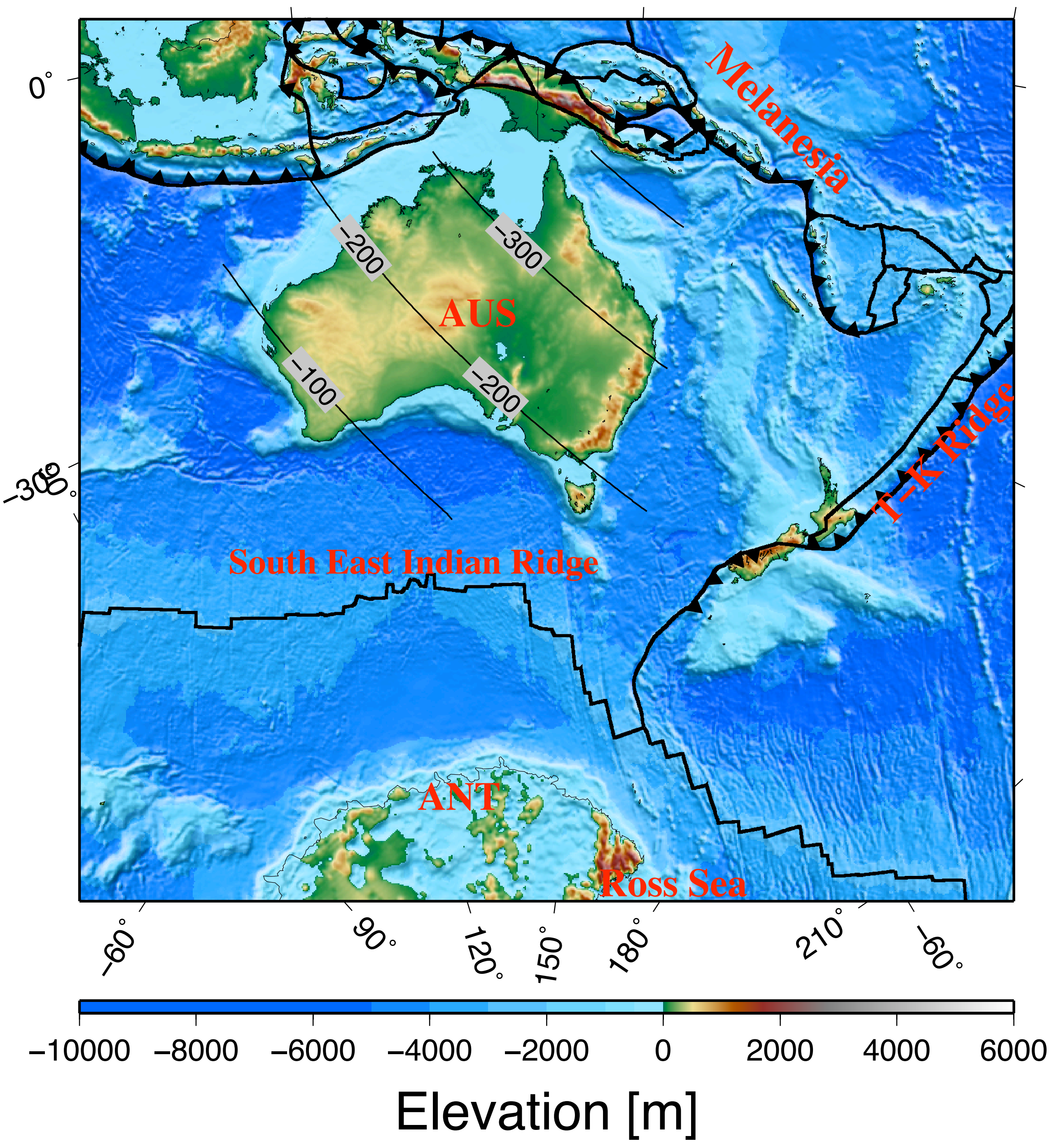

Melanesia
AUS
−300
−200
−200
−100
T–K Ridge
South East Indian Ridge
ANT
Ross Sea
0°
−30°
−60°
90°
120°
150°
180°
210°
−60°
−10000
−8000
−6000
−4000
−2000
0
2000
4000
6000
Elevation [m]

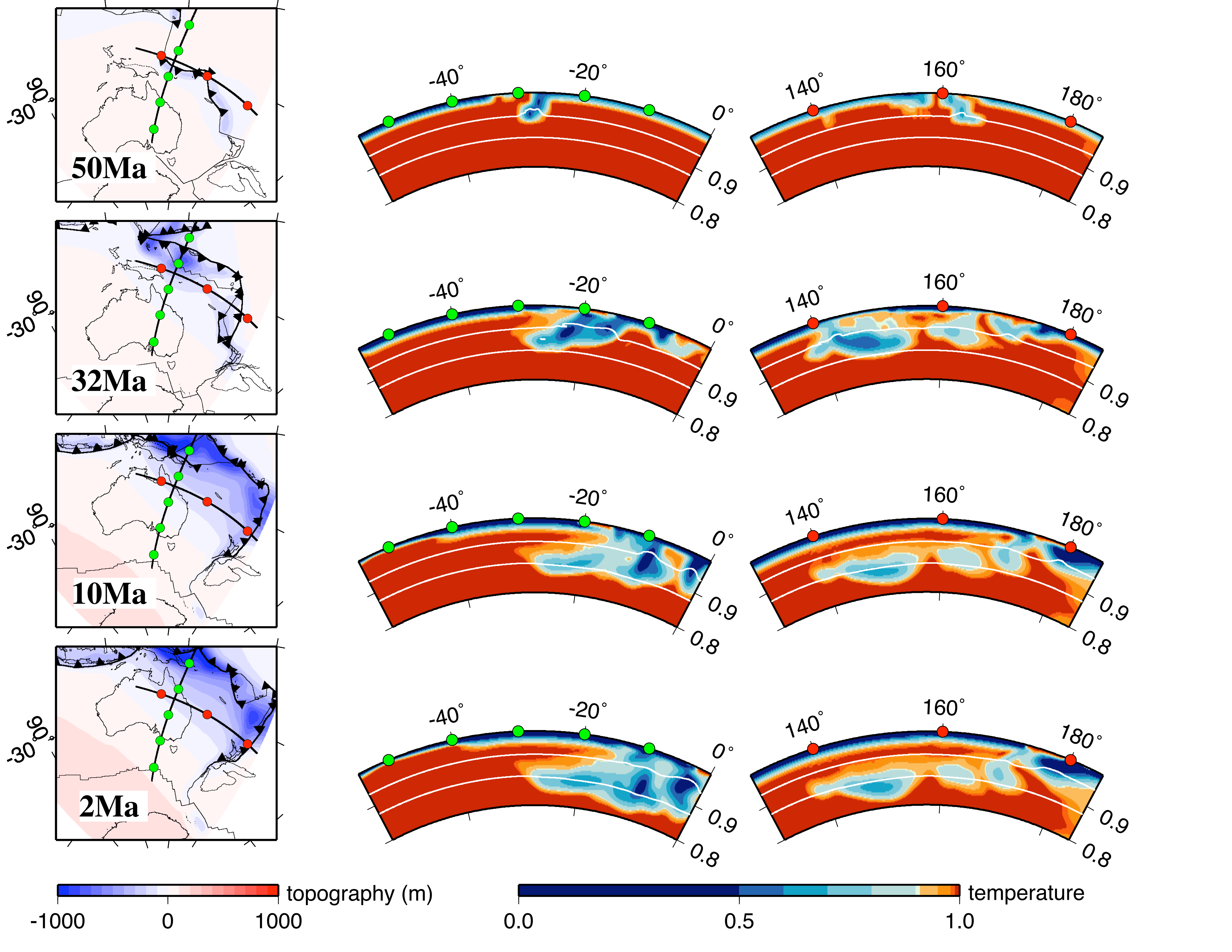

50Ma
32Ma
10Ma
2Ma
-30°
90°
-40°
-20°
0°
0.9
0.8
140°
160°
180°
-1000
0
1000
topography (m)
0.0
0.5
1.0
temperature

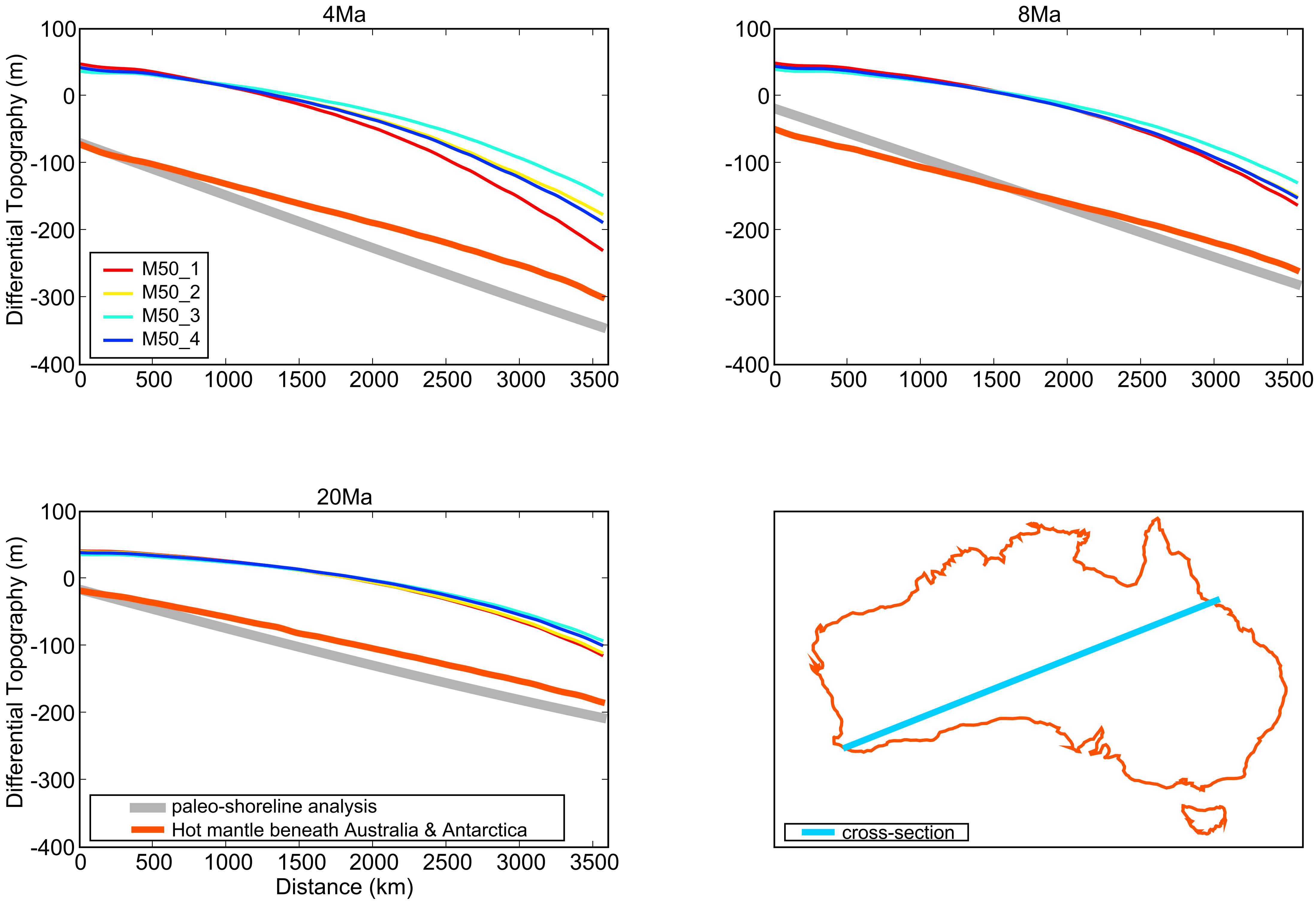

4Ma
8Ma
20Ma
Differential Topography (m)
100
0
-100
-200
-300
-400
0
500
1000
1500
2000
2500
3000
3500
Distance (km)
M50_1
M50_2
M50_3
M50_4
paleo-shoreline analysis
Hot mantle beneath Australia & Antarctica
cross-section

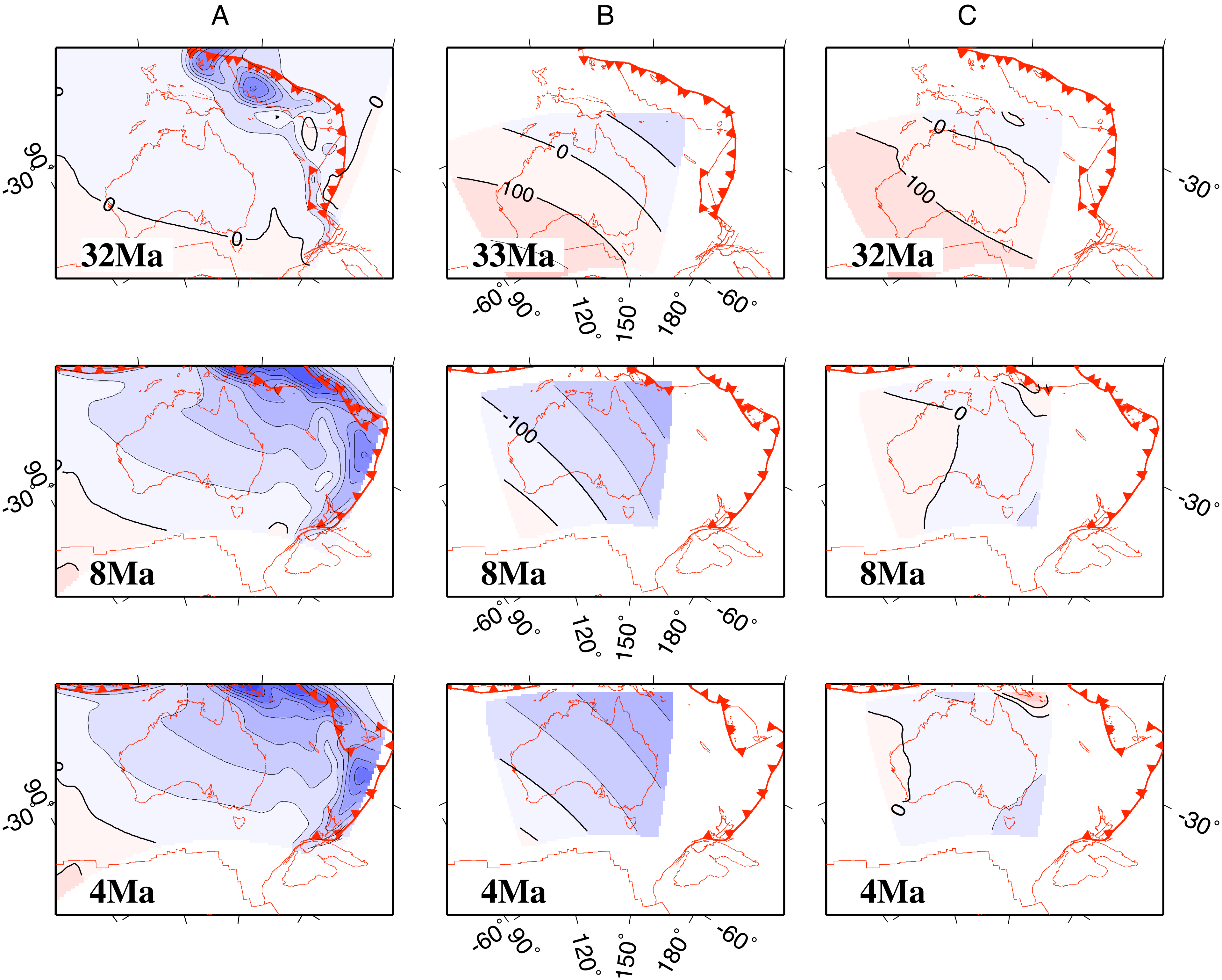

A
B
C
32Ma
33Ma
32Ma
8Ma
8Ma
8Ma
4Ma
4Ma
4Ma
0
100
-100
-30°
90°
-60°
120°
150°
180°
-60°
30°

APPENDIX

Figure A1:

Surface dynamic topography (left) since the Eocene shows progressively increasing subsidence in the northeast of Australia as the continent drifts towards the subduction zones. Reconstructed continents and plate boundaries show the position of fossil subduction zones since the Eocene. Temperature cross-sections (right) since the Eocene shows slabs accumulating beneath the northeastern margin of Australia and beneath the Tasman Sea. Temperature cross-sections are plotted with non-dimensional depths and are overlain by the 660 and 410 phase changes, which are deflected by temperature anomalies. This model topography shows the case with 75°C (5%) hotter than average mantle (1500 °C) beneath the Antarctic continent.

Figure A2:

The location of data used in the paleo-shoreline analysis study [*DiCaprio et al.*, 2009a]. Circles indicate boreholes. Erosional areas are indicated by squares. Six basins are selected (white). Inset plots show a profile (black line) with the shelf break at 200 m depth (grey line). Vertical tick marks are at 1000 m intervals in each profile. The extent of the 200 m isobath is shaded grey.

1. NUMERICAL MODELS

1.1 Governing equations

We use the finite element package *CitcomS Version 2.2* [*Tan et al.*, 2006; *Zhong et al.*, 2000] from the Computational Infrastructure for Geodynamics (CIG) (http://geodynamics.org). We treat the mantle as an incompressible viscous fluid with thermal mantle convection described by the conservation of mass, momentum and energy. These equations are solved in a spherical shell while making the Boussinesq approximation. The following equations are in the non-dimensional form where the summation over spatial indices i and j and time, t is implicit:

$$u_{i,i} = 0 \qquad (1)$$

$$-P_{,i} + (\eta u_{i,j} + \eta u_{j,i})_{,j} + \delta\rho g \delta_{ir} = 0 \qquad (2)$$

$$T_{,t} + u_i T_{,i} = \kappa T_{,ii} + H \qquad (3)$$

Where u_i is the velocity, P is the dynamic pressure, $\delta\rho$ is the density anomaly, g is the gravitational acceleration, η is the viscosity, T is the temperature, κ is the thermal diffusivity, and H is the heat production (assumed to vanish over the limited duration of our models).

The models include buoyancy forces associated with phase transitions between the upper and lower mantle, compositional variations and temperature. These density anomalies are given by:

$$\delta\rho = -\alpha\rho_0(T - T_1) + \delta\rho_{ph}\Gamma + \delta\rho_{ch}C \qquad (4)$$

where $\delta\rho_{ph}$ is the density jump across the phase change, Γ is the phase function, $\delta\rho_{ch}$ is the density difference between two compositions, C is the composition, α is the thermal expansivity, ρ_0 is the reference density, and T_1 is the surface temperature.

The mantle reference Rayleigh number is:

$$R_a = \frac{\rho_0 g \alpha \Delta \mathrm{T} R_0^3}{\kappa \eta_0} \qquad (5)$$

where κ is the thermal diffusivity, $\Delta\mathrm{T}$ is the superadiabatic temperature drop, η_0 is the reference dynamic viscosity, and R_0 is the radius of the earth. Parameters that are held constant are summarized in Table 1 while the non-dimensionalisation is described in Appendix 3.2.

Dynamic topography h, results from the vertical component of stress (σ_{rr}):

$$h = \frac{\sigma_{rr}}{\Delta\rho g} \qquad (6)$$

where $\Delta\rho$ is the density difference between mantle and the density of the overlying medium.

1.2 Model geometry and resolution

The models use coupled *CitcomS* solvers [*Tan et al.*, 2006] that allows the velocity and pressure field of a global low-resolution model to be used as the boundary conditions on the embedded solver. This provides more natural side and bottom boundary conditions on the regional solver than could be obtained with reflecting or periodic boundary conditions. Our global solver has the surface velocity imposed while the bottom boundary condition is no slip. Our regional model covers most of the present day Indo-Australian plate and part of the Pacific plate.

The globe is divided into 12 caps, containing 33 nodes in the two map and radial directions. The global model has a surface resolution of about 274 km extending from the surface to the core mantle boundary with a radial resolution of 87 km. The regional model consists of one cap with 247 nodes in the latitude and longitude directions and 65 nodes in the radial direction; the resolution at the surface is 64 km in longitude by 40 km in latitude, while extending from 64 km to 2250 km depth with a radial resolution of 33 km.

CitcomS uses regional meshes that are bounded by lines of constant latitude and longitude. During the Cretaceous, Australia was located close to the south pole so that if we choose a domain during the Cretaceous, the mesh would have been condensed at the pole. To avoid pole-refined meshing, we work in a reference frame that is rotated to the equator. This reference frame is defined by an initial rotation that is introduced at the root of the rotation tree hierarchy. We define the center of the region of interest as $135\,°E$, 37.5 $°S$ rotated to the equator. All relative plate motions remain invariant because all plates move relative to the root of the rotation tree hierarchy.

1.3 Mantle rheology

The viscosity of the mantle is strongly dependent on pressure, stress (strain rate), temperature, water, melt, grain size and composition [*Ranalli*, 1995]. However, including all these parameters in large-scale models is not currently feasible. Our models have a Newtonian viscosity that has temperature, depth, composition and position dependencies. The mantle is divided into four layers: lithosphere (0-100 km), upper mantle (100-410 km), transition zone (410-670 km), lower mantle (670-2880 km) and the viscosity of each layer is varied between models.

The temperature dependence of viscosity is:

$$\eta = \eta_0 e^{\left(\frac{A_e}{T+A_T} - \frac{A_e}{1+A_T}\right)} \qquad (7)$$

where η_0 is the reference viscosity, A_e is an effective non-dimensional activation energy, A_T is the temperature offset of 0.1 in each layer. The viscosity variation across the domain is between $2\times10^{19}\,Pas$ and $2\times10^{23}\,Pas$, consistent with observations of seismic strain rates [*Billen et al.*, 2003].

1.4 Variable phase change parameters

The transition zone is bounded in depth by two phase transitions that have both a Clapeyron slope and a density change. Recent studies suggest the Clapeyron slope at the 410 km phase change is between 2 and 4.0 MPa/K [*Katsura and Ito*, 1989; *Katsura et al.*, 2004; *Morishima et al.*, 1994]. The density difference associated with the 410 km phase change is approximately 100 kg/m^3 [*Bina and Helffrich*, 1994]. The Clapeyron slope at the 660 km phase change is between -0.5 and -4 MPa/K [*Fei et al.*, 2004; *Irifune et al.*, 1998; *Ito and Takahashi*, 1989; *Katsura et al.*, 2003; *Litasov et al.*, 2005]. The density difference at the 660 km phase change is about 236 kg/m^3 [*Ita and Stixrude*, 1992].

The Clapeyron slope of the phase changes bounding the transition zone influences the magnitude of surface topography. A steeper Clapeyron slope at the 410 km phase change (olivine to spinel) results in a greater downward body force driving flow within the cold slab and produces a larger effect on surface topography. By contrast, a steeper Clapeyron slope at the 660 km phase change (spinel to perovskite-magnesiowüstite) inhibits flow and results in less dynamic surface topography. We alter the phase change parameters while ensuring they are consistent with seismological observations and high-pressure experiments. The values used in each model are listed in Table 2.

1.5 Tracers

We use passive tracers to map the motion of Pacific and Indian mantle domains for models that start at 140 Ma. We use active tracers within the continental lithosphere to provide buoyancy and within the mantle wedge to lower the viscosity. The area of the Indian and Pacific mantle domains is delimited by the initial slab location and dip extending to the CMB on the eastern margin of Australia. To the east of the slab is the Pacific mantle domain and to the west is the Indian mantle domain. The extent of all tracers is limited by the regional box boundaries with 18 tracers per element.

Continental stability is maintained through compositionally buoyancy that tends to counteract the negative buoyancy of the continental lithosphere [*Jordan*, 1979] and use buoyant tracers to simulate this process. The average density beneath the continental cratonic crust is 3300 kg/m3 [*Dziewonski and Anderson*, 1981] [*Kaban et al.*, 2003] and we use an average density of 3500 kg/m3 within the asthenosphere. We define the buoyancy of continental lithosphere using the ratio method [*McNamara and Zhong*, 2004]:

$$B = \frac{Ra_c}{Ra} \text{ where } Ra_c = Ra\frac{\delta\rho_c}{\rho_0} \qquad (8)$$

The distribution of continental tracers is defined by continental crust and arc fragments from oceanic paleo age grids [*Müller et al.*, 2008b] over a depth of 180 km based on an average seismic depth of cratonic and Phanerozoic lithospheric elements in Australia [*Kennett*, 2003].

During subduction water is released into the upper 200 km of the mantle wedge from the downgoing slab, primarily from hydrated basalts [*Peacock*, 1990; *Ranero et al.*, 2003] and a thin veneer of pelagic sediments. Due to the presumed high concentrations of water and melt in the mantle wedge, the viscosity of the mantle wedge may be reduced by at least an order of magnitude compared to the surrounding asthenosphere [*Baker-Hebert et al.*, 2009; *Billen and Gurnis*, 2001]. This low viscosity can significantly reduce the magnitude of negative dynamic topography and the geoid by decreasing the coupling between the slab and the overriding plate [*Billen et al.*, 2003].

We use tracers to reduce the viscosity within the mantle wedge by a factor of 10 compared to the surrounding asthenosphere. The spatial distribution of mantle wedge tracers is defined by the initial slab location and dip. The depth extent of low seismic velocities assumed to be associated with the low viscosity wedge are typically 150 km above the slab but may extend to 400 km depth below the backarc [*Wiens and Smith*, 2003]. Our wedge extends from the surface to 400 km with a lateral extent of 350 km for a slab with a 50° dip.

2. ASSIMILATED DATA

2.1 Plate Kinematics

Plate motion is imposed as a velocity boundary condition using a model of continuously evolving plate boundaries whose motions are determined in a moving hotspot reference frame. We use *GPlates* software [*Boyden et al.*, 2009; *Gurnis et al.*, 2009] to reconstruct rigid plates with continuously evolving plate boundaries back to 140 Ma. Plate boundaries were used to create closed plate polygons [*Gurnis et al.*, 2009], which define the instantaneous plate velocity at 1 Myr time increments on both the global and regional *CitcomS* meshes.

Plate boundaries consist of mid-ocean ridges, subduction zones and transform faults. The position of mid-ocean ridges is found using the half-stage rotation reconstructed from magnetic lineations and the relative rotation between the two diverging plates. Fracture and subduction zones were positioned according to common reconstructions and reported preserved arc materials (Appendix 3). The rotation of these subduction zones is based on the overriding plate where no other rotation has been determined. Our reconstructions use a moving hotspot absolute plate motion reference frame [*O'Neill et al.*, 2003] from 100 Ma to the present; they use a fixed hotspot reference frame from 140 to 100 Ma [*Müller et al.*, 2008a]. The global plate motions are described by relative plate motion models summarized by Müller et al., [2008a].

2.2 Seafloor age

The reconstructed ages of the ocean floor [*Müller et al.*, 2008b], consistent with the continuously closed plate model, is assimilated into the models as a surface temperature boundary condition every 1 Myr. We use a half-space model to calculate the temperature based on the age of the oceanic crust:

$$T^{HS} = T_s + (T_m - T_s) erf\left(\frac{y}{2\sqrt{\kappa t}}\right) \qquad (9)$$

where T_s is the surface temperature (here set to non-dimensional value of 0), T_m is the ambient mantle temperature, t is time, and y is the depth. Temperature is assimilated as a linear function of depth, y , with a cutoff depth (y_p) of 80 km:

$$T_{i+1} = aT_i + (1-a)T_{i+1}^{HS} \text{ where } a = \begin{cases} \dfrac{y}{y_p} & y < y_p \\ 1 & y \geq y_p \end{cases} \qquad (10)$$

where T_i is the model temperature at timestep i and T_{i+1}^{HS} is the temperature found from the half space cooling model.

2.3 Backarc basins

Subduction-induced flow caused by the downgoing plate produces a net upward suction force on the slab that is thought to be balanced by the gravitational body force of the slab [*Stevenson and Turner*, 1977; *Tovish et al.*, 1978]. However, in purely viscous models, the broadening of the slab produces an overwhelming suction force causing the slab to be pulled up towards the overriding plate [*Christensen*, 1996; *Manea and Gurnis*, 2007]. The coupling of the slab to the overriding plate is resolved when a more realistic mantle wedge rheology is included into dynamic models [*Billen and Hirth*, 2007; *Manea and*

Gurnis, 2007] which is suitable for higher resolution, detailed models of subduction zone dynamics. However, in larger scale models, the slab suction problem can be resolved by removing the overriding plate and applying a velocity in the backarc that is trench perpendicular towards the converging margin [*Christensen*, 1996; *Tan et al.*, 2002]. Here we set the backarc region to ambient mantle temperature and impose a backarc velocity in order to insert a realistic slab into the upper mantle. The amplitude of this imposed velocity within the backarc is approximately equal but opposite to the velocity of the downgoing plate at the trench.

2.4 Initial slab parameters

We thermally prescribe a subducting slab as an initial condition. The slab has either a deep dip of 30° or 50° and is vertical in the lower mantle. The temperature profile of the slab is symmetric about its center, set to 0. The temperature gradient from its center is calculated using the half-space cooling model (equation 8), the age of the sea floor sampled at the trench, and the distance from the center of the slab.

We impose the slabs at 50 Ma at the reconstructed subduction zones surrounding the Australian continent in order to investigate the large scale, progressive tilt of the continent since the Eocene.

During the early Eocene NE-dipping subduction was located north of New Caledonia [*Aitchison et al.*, 1995; *Cluzel et al.*, 2001; *Crawford et al.*, 2003; *Spandler et al.*, 2005] producing the Eocene volcanic arc (Loyalty Ridge). This subduction may have been active since the Late Cretaceous [*Crawford et al.*, 2003; *Eissen et al.*, 1998; *Schellart et al.*, 2006] and may have continued southward into the Norfolk Basin along the Three Kings Ridge [*DiCaprio et al.*, 2009b; *Meffre et al.*, 2006; *Mortimer et al.*, 2007]. We place an initial slab to the east of New Caledonia and extending into the Norfolk Basin. The slab extends into the upper mantle to 400 km depth.

Between 50 and 45 Ma southwest-dipping subduction at the Melanesian arc was initiated [*Gaina and Müller*, 2007; *Hall*, 2002]. This subduction was preceded by Ndipping subduction north of Australia. We place an initial slab at the Melanesian arc and assume that the initial slab extends to 300 km depth.

3. MODELING PARAMETERS

Table 1: Parameters held constant within the models

Parameter	**Notation**	**value**
Reference mantle density	ρ_0	$3500\,kg/m^3$
Gravity	g	$10\,m/s^2$
Temperature of the surface	T_0	$0\,°C$
Change in temperature from the CMB to the surface	ΔT	$1500\,°C$
Radius	R_0	$6371000\,m$
Coefficient of thermal expansion	α	$2\times10^{-5}\ K^{-1}$
Thermal diffusivity	κ	$1\times10^{-6}\ m^2/s$
Reference viscosity	η_0	$2\times10^{21}\ Pas$
Rayleigh number	$R_a = \frac{\rho_0 g \alpha_0 \Delta T R_0^3}{\kappa_0 \eta_0}$	$R_a = 1.3576\times10^{+08}$

Table 2: Geodynamic models and properties

Model Name	Non-dimensional Viscosity layers	Dip	Start age	Slope 410 (MPa/K)	Slope 660 (MPa/K)
M1	100,1,5,10	50	50	4	-2
M2	100,1,5,10	50	50	4	-4
M3	100,1,5,10	50	50	2	-4
M4	100,1,5,10	50	50	2.9	3

3.2 Dimensional and non-dimensional parameters used in models

3.2.1 Reference Rayleigh Number

R_a is the whole mantle Rayleigh number which is defined as:

$$R_a = \frac{\rho_0 g \alpha_0 \Delta T R_0^3}{\kappa_0 \eta_0}, \quad R_a = 1.3576 \times 10^{+08}$$

3.2.2 Phase change

The buoyancy of the transition zone is defined by the Clapeyron slope and the density change. The density change is expressed within the phase change Rayleigh number.

Phase change Rayleigh number

The density change at the 410 km transition (olivine – wadsleyite) is between 3% and 5%. The density change at the 660 km transition (ringwoodite-perovskite) is between 7% - 9.3 % (Dziewonski and Anderson, 1981;Kennett, et al., 1995;Weidner and Wang., 1998). The Rayleigh number of the phase change is defined as: $R_{ph} = R_a\left(\frac{\Delta\rho_{ph}}{\rho_0}\right) = \frac{\Delta\rho_{ph} g R^3}{\eta\kappa}$

Table 3: Rayleigh numbers used at the 660 km and 410 km transition zones

Mineral change	**% $\Delta\rho$**	$\Delta\rho\left(kgm^{-3}\right)$	R_{ph}	**Reference**

410 km Olivine-Wadsleyite	3.0-5.7	100	R_{ph410} 1.293e+08	(Bina and Helffrich, 1994)
660 km Ringwoodite-Perovskite	7.0-9.3	236	R_{ph660} 3.05e+08	(Akaogi and Ito, 1999)

3.2.3 Clapeyron slope

The clapeyron slope at the 410 km transition (olivine-wadsleyite) is 2.5 – 4.0 MPa/K (Katsura and Ito, 1989;Katsura, et al., 2004;Morishima, et al., 1994). The clapeyron slope at the 660 km transition (ringwoodite-perovskite) is between -0.5 and -3.0 MPa/K (Fei, et al., 2004;Irifune, et al., 1998;Ito and Takahashi, 1989;Katsura, et al., 2003;Litasov, et al., 2005). The clapeyron slope is defined as $\frac{d\mathrm{P}}{d\mathrm{T}}$ and is non-dimensionalised using $\gamma = \frac{\rho_0 g_0 R_0}{\Delta \mathrm{T}} \gamma'_{ph}$ where γ' is the non-dimensionalised slope.

Table 4: This is an example of the ranges and values used for the 410 km and 660 km Clapeyron slopes

Mineral change	γ **(MPa/K)**	γ **used**	γ'	**Reference**
410 km Olivine-Wadsleyite	2.5 to 4.0	4.0	0.0269	(Katsura and Ito, 1989;Katsura, et al., 2004;Morishima, et al., 1994)
660 km Ringwoodite-Perovskite	-0.5 to -3.0	-2.0	-0.0135	(Fei, et al., 2004;Irifune, et al., 1998;Ito and Takahashi, 1989;Katsura, et al., 2003;Litasov, et al., 2005)

3.2.4 Temperature change of phase change

The temperature change at the phase change is described by $\mathrm{T}_0 = \Delta\mathrm{T}\mathrm{T}'_0$ where $\mathrm{T}'_0 = 0.1821$. The temperature is non-dimensionalised by $\mathrm{T} = \Delta\mathrm{T}(\mathrm{T}' + \mathrm{T}'_0)$.

Mineral change	$T(C^\circ)$	**Reference**	T

410 km Olivine-Wadsleyite	1673-1923	(Bina and Helffrich, 1994)	0.9332
660 km Ringwoodite-Perovskite	1673-1923	(Bina and Helffrich, 1994)	0.9332

3.2.5 Viscosity

Viscosity in our models is both temperature and depth dependent. Viscosity is non-dimensionalised using $\eta' = \frac{\eta}{\eta_0}$ where η_0 is the reference viscosity $\eta_0 = 2e^{+21}$, and η is dimensionalised viscosity. The minimum viscosity is set to 0.01 (2×10^{19}) and we limit the maximum viscosity to be 2×10^{23} in order for modeled slab viscosity to be consistent with observations of dynamic topography and the geoid in active subduction zones (Billen, et al., 2003). We impose a layered viscosity mantle. It is thought that the upper mantle is weak in order to account for post glacial rebound and geoid anomalies (Hager and Richards, 1989) and (Mitrovica and Forte 1997) .

3.2.6 Temperature dependence of viscosity

The temperature dependence of viscosity is governed by the following viscosity law:

$Vis\cos ity = \eta_0 e^{\left(\frac{A_e}{T+A_T} - \frac{A_e}{1+A_T}\right)}$ where η_0 is the reference viscosity, η_e is the activation energy, η_T is the temperature offset of each layer. This has the effect of producing structures with shorter wavelengths (Zhong*, et al.*, 2000). We use the following activation energy and temperature offset for each layer:

Table 5: Activation energy and temperature offset for each layer

$A_{e\,0-100}$	$A_{e100-410}$	$A_{e\,410-660}$	$A_{e\,660-CMB}$
11	11	11	11
$A_{t\,0-100}$	$A_{t100-410}$	$A_{t410-660}$	$A_{t660-CMB}$
0.1	0.1	0.1	0.1

3.2.7 Cratons and compositional buoyancy

The density change due to a chemical change of viscosity is given by $\delta\rho = \delta\rho_{ch} C$. The typical density of the lithospheric mantle beneath cratons is: $\rho_{ch} = 3300$. $\delta\rho_{ch}$ is the density contrast between different chemical components, C is the composition (some factor), $\delta\rho$ is the thermal change in density.

$$\delta\rho = \rho_0 \Delta T \alpha$$
$$\delta\rho = 3500 \times 1500 \times 2 \times 10^{-5}$$
$$\delta\rho = 105$$
$$\delta\rho_{ch} = 3500 - 3300 = 200$$
$$C = \frac{\delta\rho}{\delta\rho_{ch}} = \frac{105}{200} = 0.5250$$

3.2.8 The Chemical Rayleigh number and buoyancy ratio

The chemical Rayleigh number is given by:

$$Rac = Ra \frac{\delta\rho_{ch}}{\rho_0}$$
$$Rac = \frac{\Delta\rho g R^3}{\eta\kappa}$$
$$Rac = \frac{200 \times 10 \times 6371000^3}{1 \times 10^{-6} \times 2 \times 10^{21}}$$
$$Rac = 2.5860 \times 10^8$$

The buoyancy ratio (B), is a non-dimensional quantity which is the ratio of chemical to thermal buoyancy (McNamara and Zhong, 2004).

$$B = \frac{Rac}{Ra}$$
$$B = \frac{\Delta\rho_{ch}}{\Delta\rho}$$
$$B = \frac{2.586 \times 10^{+08}}{1.3576e^{+08}}$$
$$B = 1.9048$$

Aside:

$$\alpha = \frac{1}{V}\frac{\partial V}{\partial T}$$

$$V = \frac{m}{\rho}$$

$$\frac{\partial V}{\partial T} = m\frac{\partial}{\partial T}\left(\frac{1}{\rho}\right)$$

$$\frac{\partial V}{\partial T} = m(-1)\rho^{-2}\frac{\partial \rho}{\partial T}$$

$$\alpha = \frac{\rho}{m}m(-1)\rho^{-2}\frac{\partial \rho}{\partial T}$$

$$\alpha = \rho^{-1}\frac{\partial \rho}{\partial T}$$

$$\Delta\rho = \rho_0 \Delta T \alpha$$

References

Aitchison, J. C., et al. (1995), Eocene arc-continent collision in New Caledonia and implications for regional southwest Pacific tectonic evolution, *Geology*, *23*, 161-164.

Baker-Hebert, L., et al. (2009), Emergence of a low-viscosity channel in subduction zones through the coupling of mantle flow and thermodynamics, *Earth and Planetary Science Letters*, *278*(3-4), 243-256.

Billen, M., and G. Hirth (2007), Rheologic controls on slab dynamics, *Geochemistry Geophysics Geosystems*, *8*(Q08012).

Billen, M. I., and M. Gurnis (2001), A low viscosity wedge in subduction zones, *Earth and Planetary Science Letters*, *193*(1-2), 227-236.

Billen, M. I., et al. (2003), Multiscale dynamics of the Tonga–Kermadec subduction zone, *Geophysical Journal International*, *153*, 359-388.

Bina, C. R., and G. Helffrich (1994), Phase transition Clapeyron slopes and transition zone seismic discontinuity topography, *Journal of Geophysical Research*, *99*(B8), 15,853-815,860.

Boyden, J., et al. (2009), Next-generation plate-tectonic reconstructions using GPlates, in *Geoinformatics: Cyberinfrastructure for the Solid Earth Sciences*, edited by G. R. Keller and C. Baru, Cambridge University Press, in preparation, Cambridge.

Christensen, U. R. (1996), The influence of trench migration on slab penetration into the lower mantle, *Earth and Planetary Science Letters*, *140*(1-4), 27-39.

Cluzel, D., et al. (2001), Tectonic accretion and underplating of mafic terranes in the late Eocene intraoceanic fore-arc of New Caledonia (Southwest pacific):Geodynamic implications., *Tectonophysics*, *340*, 23–59.

Crawford, A. J., et al. (2003), 120 to 0 Ma tectonic evolution of the southwest Pacific and analogous geological evolution of the 600 to 220 Ma Tasman Fold Belt system., in *Evolution and dynamics of the Australian Plate*
, edited by R. R. Hills and R. D. Muller, pp. 377-397, Geological Society of Australia Special Publication 22 and Geological Society of America Special Paper 372.

DiCaprio, L., et al. (2009a), Long-wavelength tilting of the Australian continent since the Late Cretaceous, *Earth and Planetary Science Letters*, *278*, 175-185.

DiCaprio, L., et al. (2009b), Linking active margin dynamics to overriding plate deformation: Synthesizing geophysical images with geological data from the Norfolk Basin., *Geochemistry Geophysics Geosystems*, *10*.

Dziewonski, A. M., and D. L. Anderson (1981), Preliminary reference Earth model, *Physics of the Earth and Planetary Interiors*, *25*, 297–356.

Eissen, J.-P., et al. (1998), Geochemistry and tectonic significance of basalts in the Poya Terrance, New Caledonia, *Tectonophysics*, *284*, 203-219.

Fei, Y., et al. (2004), Experimentally determined postspinel transformation boundary in Mg2SiO4 using MgO as an internal pressure standard and its geophysical implications. , *Journal of Geophysical Research*, *109*.

Gaina, C., and R. D. Müller (2007), Cenozoic tectonic and depth/age evolution of the Indonesian gateway and associated back-arc basins, *Earth Science Reviews*, *in press*.

Gurnis, M., et al. (2009), Global Plate Reconstructions with Continuously Closing Plates, *Geochemistry, Geophysics, Geosystems submitted*, *Special theme "Plate Reconstructions, Mantle Convection, and Tomography Models: A Complementary Vision of Earth's Interior"*.

Hall, R. (2002), Cenozoic geological and plate tectonic evolution of SE Asia and the SW Pacific: computer-based reconstructions, model and animations, *Journal of Asian Earth Sciences*, *20*, 353-431.

Irifune, T., et al. (1998), Postspinel phase boundary in Mg2SiO4 determined by in situ X-ray measurement., *Science*, *279*, 1698–1700.

Ita, J. J., and L. Stixrude (1992), Petrology, elasticity, and composition of the mantle transition zone,, *Journal of Geophysical Research*, *97*, 6849-6866.

Ito, E., and E. Takahashi (1989), Post-spinel transformations in the system Mg2SiO4-Fe2SiO4 and some geophysical implications, *Journal of Geophysical Research*, *94*, 10637–10646.

Jordan, T. H. (1979), Mineralogies, densities and seismic velocities of garnet lherzolites and their geophysical implications. , in *The mantle sample: inclusions in kimberlites and* *other volcanics*, edited by F. R. Boyd and H. O. A. Meyer, pp. 1-14, Proc. 2nd Intern. Kimberlite Conf. .

Kaban, M. K., et al. (2003), Density of the continental roots: compositional and thermal contributions, *Earth and Planetary Science Letters*, *209*(1-2), 53-69

Katsura, T., and E. Ito (1989), The system Mg2SiO4-Fe2SiO4 at high pressures and temperatures:precise determinations of stabilities of olivine, modified spinel, and spinel, *Journal of Geophysical Research*, *94*(15), 663–670.

Katsura, T., et al. (2003), Post-spinel transition in Mg2SiO4 determined by high p-t in-situ X-ray diffractometry., *Physics of the Earth and Planetary Interiors*, *136*, 11-24.

Katsura, T., et al. (2004), Olivinewadsleyite transition in the system (Mg,Fe)2SiO4., *Journal of Geophysical Research*, *109*(B02209).

Kennett, B. L. N. (2003), Seismic structure in the mantle beneath Australia, in *Evolution and Dynamics of the Australian Plate*, edited by R. R. Hillis and R. D. Muller, pp. 7-23, Geological Society of Australia Special Publication 22 and Geological Society of America Special Paper 372, Sydney.

Litasov, K., et al. (2005), In situ X-ray diffraction study of postspinel transformation in a peridotite mantle: implications for the 660-km discontinuity., *Earth and Planetary Science Letters*, *238*, 311-328.

Manea, V., and M. Gurnis (2007), Subduction zone evolution and low viscosity wedges and channels, *Earth and Planetary Science Letters*, *264*, 22–45.

McNamara, A. K., and S. Zhong (2004), Thermochemical structures within a spherical mantle: Superplumes or Piles?, *Journal of Geophysical Research*, *109*(B07402).

Meffre, S., et al. (2006), Arc-continent collision forming a large island between New Caledonia and New Zealand in the Oligocene., paper presented at Australian Earth Science Convention., Melbourne.

Morishima, H., et al. (1994), The phase boundary between α- and β-Mg2SiO4 determined by in situ X-ray observation., *Science*, *265*, 1202–1203.

Mortimer, N., et al. (2007), Oligocene-Miocene tectonic evolution of the South Fiji Basin and Northland Plateau, SW Pacific Ocean: evidence from petrology and dating of dredged rocks., *Marine Geology.*, *237*, 1–24.

Müller, R. D., et al. (2008a), Age, spreading rates and spreading asymmetry of the world's ocean crust, *Geochemistry, Geophysics, Geosystems*, *9*(Q04006).

Müller, R. D., et al. (2008b), Long-Term Sea-Level Fluctuations Driven by Ocean Basin Dynamics, *Science*, *319*(5868), 1357 - 1362.

O'Neill, C., et al. (2003), Geodynamic implications of moving Indian Ocean hotspots, *Earth And Planetary Science Letters*, *215*(1-2), 151-168.

Peacock, S. (1990), Fluid processes in subduction zones, *Science*, *248*, 329–337.

Ranalli, G. (1995), *Rheology of the earth*, 2 ed., Chapman & Hall, London.

Ranero, C., et al. (2003), Bending-related faulting and mantle serpentinization at the Middle America trench, *Nature*, *425*, 367–373.

Schellart, W. P., et al. (2006), A Late Cretaceous and Cenozoic reconstruction of the Southwest Pacific region: Tectonics controlled by subduction and slab rollback processes, *Earth-Science Reviews*, *76*(3-4), 191-233.

Spandler, C., et al. (2005), Late cretaceous-tertiary tectonics of the southwest pacific: Insights from u-pb sensitive, high-resolution ion microprobe (shrimp) dating of eclogite facies rocks from new caledonia, *Tectonics*, *24*.

Stevenson, D. J., and J. S. Turner (1977), Angle of subduction, *Nature*, *270*, 334-336.

Tan, E., et al. (2002), Slabs in the lower mantle and their modulation of plume formation, *Geochemistry Geophysics Geosystems*, *3*(11), 1067.

Tan, E., et al. (2006), GeoFramework: Coupling multiple models of mantle convection within a computational framework, *Geochemistry, Geophysics, Geosystems 7*.

Tovish, A., et al. (1978), Mantle flow pressure and the angle of subduction: non-Newtonian corner flows, *Journal of Geophysical Research*, *83*, 5892-5898.

Wiens, D. A., and G. P. Smith (2003), Seismological constraints on structure and flow patterns within the mantle wedge, in *Inside the subduction factory*, edited by J. Eiler, Geophysical Monograph, American Geophysical Union, Washington DC.

Zhong, S. J., et al. (2000), Role of temperature-dependent viscosity and surface plates in spherical shell models of mantle convection, *Journal of Geophysical Research- Solid Earth*, *105*(B5), 11063-11082.